Applied Catalysis B: Environmental 165 (2015) 419–427

Contents lists available at ScienceDirect

Applied Catalysis B: Environmental

journal homepage: www.elsevier.com/locate/apcatb

Bio-inspired design: Inner-motile multifunctional ZnO/CdS heterostructures magnetically actuated artificial cilia film for photocatalytic hydrogen evolution

Fengping Peng [a], Qiang Zhou [a], Dunpu Zhang [a], Chunhua Lu [a,*], Yaru Ni [a,b,**], Jiahui Kou [a], Jian Wang [a], Zhongzi Xu [a]

[a] State Key Laboratory of Materials-Orient Chemical Engineering, College of Materials Science and Engineering, Nanjing Tech University, Nanjing 210009, PR China
[b] Southeast University, Nanjing 210096, PR China

ARTICLE INFO

Article history:
Received 30 July 2014
Received in revised form
16 September 2014
Accepted 19 September 2014
Available online 23 October 2014

Keywords:
Biomimetic
Cilia
Magnetic materials
Photocatalytic hydrogen evolution
Z-scheme

ABSTRACT

A novel inner-motile film for photocatalytic water splitting has been designed for the first time. The inner-motile photocatalyst film is a highly elaborate machinery and mainly integrates three functional modules – magnetically actuated artificial cilia, ZnO nanowires arrays and CdS quantum dots, which can work synergistically to enhance the photocatalytic hydrogen evolution activity. Through citing magnetically actuated artificial cilia, the inner-motile film can mimic ciliary motion like nature beating cilia under a rotational magnetic field. Hence it exhibits a singular ability of microfluidic manipulation, which is helpful to solve the stubborn problem of desorption of hydrogen and promotes release of active sites. In contrast to the traditional external magnetic-stirrer technologies, the photocatalytic activity can be greatly improved. Moreover, forest-like hierarchical structured ZnO nanowires arrays have been constructed by being grafted on magnetically actuated artificial cilia, which increase the surface area and light absorption. Furthermore, the photocatalytic modules – coupled ZnO/CdS heterostructures based on the Z-scheme mechanism has been devised to enhance electron–hole separation and interfacial charge transfer, in which ZnO and CdS serve as PS II and PS I, respectively. Consequently, the H_2 evolution rates of ZnO nanowires arrays/CdS heterostructures are about 2.7 times, 2.0 times of CdS substance and ZnO nanoparticles/CdS heterostructures, respectively. The design of the inner-motile system film is based on both nature cilia and photosynthesis, which would broaden the horizon for constructing artificial photocatalyst system and provide a new working prototype for photochemical hydrogen production.

1. Introduction

Solar-driven photocatalytic water splitting for renewable production of hydrogen has been triggered by the growing energy crisis. It is acknowledged that the primary and ideal photocatalytic water splitting processes include light harvesting, photoinduced charge separation and transport, release of hydrogen from the surface of photocatalyst, which need a highly elaborate machinery to complete. However, traditional pholocatalysts are used in suspension in the form of powders [1,2], which made them hard to retrieve. Then the photocatalyst films [3–13] became the focus of research gradually. Nevertheless, traditional films are inflexible. So in traditional hydrogen production system, it has to negatively rely on external magnetic-stirrer technologies for the release of hydrogen, otherwise an infinitesimal amount of H_2 will absorb onto the surface of pholocatalyst, which may slower the evolution reaction toward hydrogen and improve the potential hazard of inverse response. However there is always no provoking thinking for effective stirring technologies all the time, so the release of hydrogen has become the inherent critical obstacle for traditional hydrogen production system.

Imagining a scene that if the photocatalytic films are inner-motile and can manipulate fluid and boost migration of bubbles autonomously, it may be possible to accelerate the release of H_2, and get rid of the bondage of inefficient external magnetic-stirrer technologies. But conventional films are inflexible and cannot meet

* Corresponding author. Tel.: +86 25 83587252; fax: +86 25 83587220.
** Corresponding author at: State Key Laboratory of Materials-Orient Chemical Engineering, College of Materials Science and Engineering, Nanjing Tech University, Nanjing 210009, PR China.
E-mail addresses: lchhnjtech@163.com, chhlu@njtech.edu.cn (C. Lu), nyr@njtech.edu.cn (Y. Ni).

http://dx.doi.org/10.1016/j.apcatb.2014.09.050
0926-3373/

the inner-motile performance requirement. So it is a big challenge to design an inner-motile photocatalyst film, which limits creative innovation.

However, inspiration was obtained from the natural cilia, the hair-like structures, which can manipulate fluid and serve as microfluidic actuators on the microscale in nature [14]. Moreover in recent years, there has been an increasing interest in developing artificial counterparts to explore strategies to drive or manipulate the flow. In addition, artificial cilia are in particular proved to be extraordinarily favoring to the fluid manipulation [14–20] through mimicking the form and function of natural beating cilia, thereby which provide an underlying solution of manipulating fluid to eliminate bubbles in the absence of external magnetic-stirrer technologies.

Recently we have reported a study on ciliary array@rG–COOH@TiO_2 (AGT) [21] and proved that the activity of degradation of tetraethylated rhodamine B (RhB) is improved to approximately 3.0 times because a motion similar to that of natural cilia accelerates interior mass transfer. Furthermore, if the singular inner-motile characteristic is cited into the photocatalytic hydrogen production system, which will be a magic key to solving desorption of H_2.

In the research of photocatalytic hydrogen evolution, Z-scheme is recognized as an ideal hydrogen evolution system. Based on the Z-scheme, many efforts have been made to develop artificial photosynthetic systems [22–26] by constructing various hybrid to mimic the separation of light-driven electron–hole pairs and keep reduction and oxidation reactions at two different reaction sites. However, traditional Z-schemes are almost studied in the form of suspension systems. And most research only focused on the functional imitation of photosynthesis and neglected the structure effort [27,28].

Herein, we adopt a self-contained design concept, and assemble an inner-motile magnetically actuated artificial cilia (magnetically cilia for short) film into the photocatalytic hydrogen production system for the first time. On the platform of this interesting inner-motile film, the Z-scheme of ZnO/CdS (ZCS) was constructed and optimized by grafting ZnO nanowire branches, which good for the enhanced effective light pathlength [8] and fast charge transport and separation [29]. Finally, the ZCS-B films were successfully prepared for efficient water splitting. Through experiment the ZCS-B film was proved as a highly elaborate machinery, which can complete the water splitting processes by a synergy of diverse complex structures and functional modules just like forest photosynthesis in nature: the flexible artificial cilia strongly favor release of hydrogen as well as multiple scattering and absorbance of light [30]; two intimately contacted semiconductors (ZnO/CdS heterostructures) without the assistance of redox mediators can realize the desirable reverse carrier transfer [22] and more powerful excited electrons holes can be remained on different counterparts for efficient hydrogen evolution; three-dimensional (3D) construction of ZnO nanowire arrays grafted on cilia are not only good for the enhanced effective light pathlength, but also for fast charge transport and separation due to high electron diffusion coefficient of ZnO nanowires [29], which could help improve the electron lifetime. Hence, the inner-motile multifunctional ZCS-B films were constructed successfully for the first time, which especially solve the long outstanding hydrogen desorption problem. Comparing with the system with traditional external magnetic-stirrer technologies, the hydrogen production efficiency of ZCS-B with singular inner-motile characteristic can be tremendously enhanced. Therefore, the nature is a fascinating source of inspiration for the development of model systems and the artificial photosynthesis will come true gradually through unremitting efforts.

2. Experimental

2.1. Materials

All the reagents were of analytical grade and were used without future purification. Distilled water was used in the whole experiment. A 2-component polydimethylsiloxane (PDMS, Sylgard 184) from Dow Corning (MI, USA) with a 10:1 base to curing agent mixing ratio was used. The cobalt (Co) powders (100–200 nm) were prepared by chemical vapor deposition method, purchased from Miyou Company. Dimethylbenzene (C_8H_{10}, ≥99.0%), zinc acetate dehydrate ($Zn(CH_3COO)_2{\cdot}2H_2O$, ≥99.0%), isopropyl alcohol (C_3H_8O, ≥99.7%), triethylamine ($(C_2H_5)_3N$, ≥99.0%), hexamethylenetetramine ($C_6H_{12}N_4$, ≥99.0%), zinc nitrate hexahydrate ($Zn(NO_3)_2{\cdot}6H_2O$, ≥99.0%), ethanol (CH_3CH_2OH, ≥99.7%), Cadmium chloride ($CdCl_2{\cdot}2.5H_2O$, ≥99.0%), sodium sulfide nonahydrate ($Na_2S{\cdot}9H_2O$, ≥98.0%), sodium sulfite anhydrous (Na_2SO_3, ≥97.0%) were purchased from Sinopharm Chemical Reagent Co., Ltd.

2.2. Preparation of magnetic cilia

It is reported that magnetic nanoparticles can form aligned nanowires inside different polymer matrix with parallel. So we prepared the magnetic cilia as follows. Typically, the 0.15 g Co powers was dispersed in the 7 g dimethylbenzene with the ultrasonic treatment for 2 min. 3 g PDMS resin was added into the suspension of Co powers and dimethylbenzene. The mixture was stirred with the motor agitator (JJ-1) at 300 r/min for 1 h. Then Sylgard-184B was added into the above mixture to form the final coating and the amount of Sylgard-184B was 10%wt of the Sylgard-184A. After stirring for 10 min, 1 ml of coatings were added into a home-made polytetrafluoroethylene (PTFE) trough (the size of trough was 20 mm × 20 mm × 3 mm). The PTFE cells were put into 900 mT perpendicular magnetic field at room temperature. After being treated for 24 h, the PTFE cells were taken out from the magnetic field and the self-supporting magnetic cilia was obtained. The schematic illustration of the structure formation of ZC-B is shown in Fig. 1a.

2.3. Preparation of ZnO magnetically cilia with 3D branched structure (ZC-B)

0.006 mol of zinc acetate dihydrate was dissolved in screwthread erlenmeyer flask containing 50 ml of isopropyl alcohol. After the solution was stirred at 80 °C for 15 min, 0.506 g

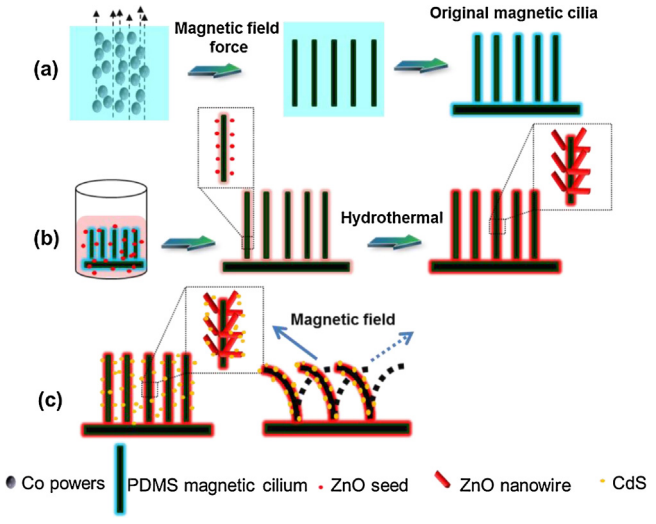

Fig. 1. Schematic illustration of the structure formation of ZCS-B.

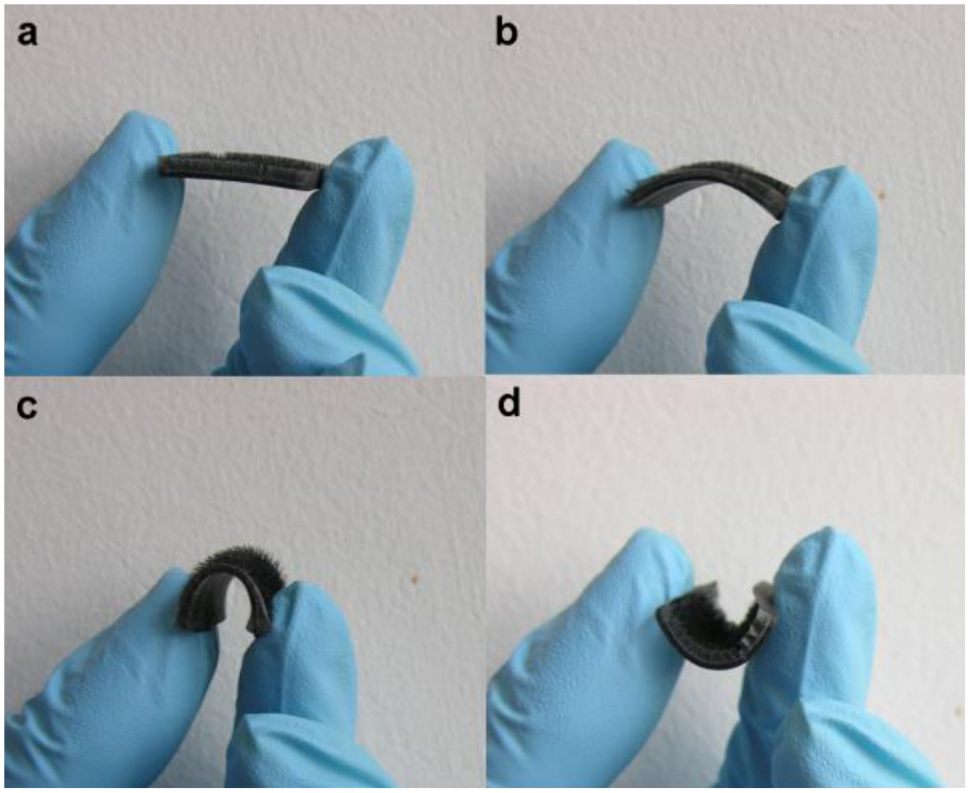

Fig. 2. The high mechanical stability and structural flexibility of the ZCS-B.

triethylamine was added drop by drop, resulting in a clear solution, which was kept at the same temperature for additional 10 min. At last a milky solution (named ZnO seed solution) was obtained and then aged at room temperature for 3 h.

ZnO growth solution was prepared as follows. 0.014 mol of hexamethylenetetramine was dissolved in 550 ml of distilled water. When dissolved fully, 0.014 mol of zinc nitrate hexahydrate was added into the solution and stirred for 24 h.

Then the magnetic cilia was dipped into the seed solution, rinsed with ethanol, heat treated at 120 °C for 1 h and then dried in air for 12 h, which process was ZnO-seeds treatment. After the seeds treatment, the magnetic cilia was put into a Teflon-lined stainless steel autoclave (60 ml capacity) with 50 ml of ZnO growth solution and heated at 90 °C for 8 h. The Teflon-lined stainless steel autoclave was cooled to room temperature naturally. After 12 h, the treated samples was removed from the growth solution, rinsed with distilled water and ethanol, at last dried in air, and labeled as ZC-B. The schematic illustration of the structure formation of ZC-B is shown in Fig. 1b.

The preparation of ZC-P was similar to the one which was used to prepare ZC-B in the absence of the seed treatment.

2.4. Preparation of ZnO/CdS heterostructures magnetically cilia film (ZCS-B)

Typical CdS quantum dots (QDs) sensitization is as follows. 0.25 mmol $CdCl_2{\cdot}2.5H_2O$ was dissolved into a 50 ml H_2O. Then ZC-B films were put into this solution for 15 min to make Cd^{2+} absorbed onto the surface of ZC-B films fully. Afterwards, a 0.1 M Na_2S solution was added dropwise into the above solution until pH = 7. Finally, the final film samples were taken out and dried at 60 °C for 24 h in air, resulting in ZnO/CdS heterostructures magnetically cilia film (ZCS-B) (Fig. 1c).

The preparation of CSC and ZCS-P was similar to the ZCS-B but magnetically cilia, ZC-P takes the place of ZC-B, respectively.

A table for the prepared samples has been given in Supplementary Material Table S1.

2.5. Characterization

The morphology and size of magnetically actuated ZCS-B films with 3D branched structure were measured by FESEM. The structure characterization of samples was performed on a SmartLab (Rigaku) thin-film diffractometer employing Cu K_α radiation (λ = 0.15406 nm) and incident angle 1.0°, with a scanning rate of 10°/min in the 2θ angle ranged from 20° to 80°. TEM and HRTEM analysis were conducted on a JEM-2010 electron microscope (JEOL, Japan) at an accelerating voltage of 200 kV. UV-Vis DRS were obtained for the prepared samples using an ultraviolet-visible-near infrared (UV-Vis-Nir) 3101 spectrophotometer (Shimadzu) with $BaSO_4$ as the reflectance sample in the wavelength ranged from 200 to 800 nm. Stereoscopic microscopy (Nikon, ZSM 745T, Japan) was used to monitor the ciliary motion in solution or air driven by rotation magnetic field. The rotational magnetic field was provided by a paired flat permanent circular magnet (neodymium, N52, Φ 25 × 5 mm), which was symmetrically placed on a variable frequency motor.

2.6. H_2 evolution measurements

H_2 evolution measurements using the prepared samples were conducted on a CEL-SPH2N photocatalytic water-splitting testing system (Fig. S1) connected with SP-6890 gas chromatograph. Typically, the measurements on a prepared film (20 mm × 20 mm × 3 mm) were carried out in a 50 ml aqueous solution containing SO_3^{2-} and S^{2-} ions (0.1 M Na_2S and 0.1 M Na_2SO_3)

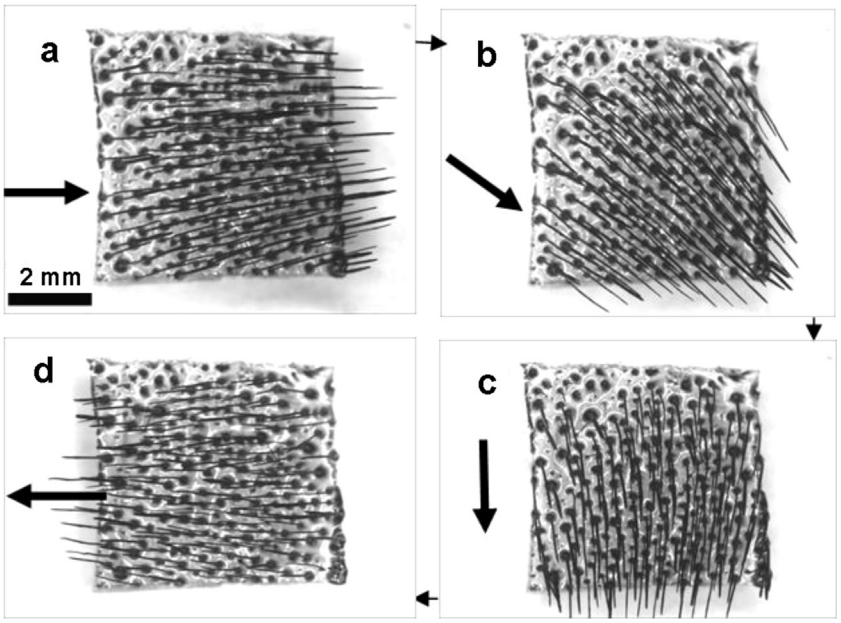

Fig. 3. Optical micrograph sequences of the magnetically actuated ZCS-B in air bending along the rotational magnetic field lines.

as sacrificial reagents under the irradiation of a 300 W xenon lamp. Before the reaction, the air in the system was removed by a pump, and the H_2 evolved for 5 h was periodically analyzed by a gas chromatograph online every 1 h.

3. Results and discussion

In the structure, the polydimethylsiloxane (PDMS) was applied to obtain the flexible substrate and provide the membrane with durability. Fig. 1 shows the schematic illustration of the structure formation of ZCS-B. Firstly, magnetic cilia were prepared successfully by a facile bottom-up approach on the basis of magnetic assembly. In the magnetic field, the cobalt (Co) particles instantaneously oriented in the magnetic field direction to form chains, while the polymer molecules remain dissolved. Dimethylbenzene as solvent of PDMS is allowed to completely evaporate at room temperature. Hence, with its evaporating, the elastomeric polymer molecules cross linked, cover the Co chains and penetrate the voids between the particles. After PDMS completely cure, magnetic cilia with a micron-sized array structure can be obtained. Afterwards, to avoid damage PDMS, the low-temperature hydrothermal growth technique is adopted and then the branched ZnO nanowires are constructed as the grafted superstructure of magnetic cilia. Finally, through typical preparation of CdS at low temperature, the desired samples (ZCS-B) were got. It is noteworthy that the as-prepared ZCS-B films inherit characteristics of original magnetic cilia, and are a kind of flexible, mechanically stable and free-standing film (Fig. 2), which profit from low-temperature operation with great care. Because of the excellent characteristics, the cilia mimics of the ZCS-B can respond to an external magnetic field by reversibly bending to any specific angle along the local magnetic field lines as shown in Fig. 3.

FESEM was detected to study the morphologies and refined structures of the ZCS-B film, as shown in Fig. 4. It can be observed that magnetic cilia process a micron-sized array structure akin to forest. The space between two sticks of cilium is about 200∼300 μm and the height of a stick of magnetic cilium is about 2.322 mm in Fig. 4a. After the seed and heat treatment, the bare rough cilia (Fig. 4b) are grafted with ZnO nanowire branches to serve as the superstructure (Fig. 4c), shaping a micronano structure. Considering the experiment process, crowded growth of ZnO nanowire branches suggest that ZnO nanocrystals formed discrete nucleation sites uniformly distributing over the entire magnetic cilia, which directed the growth of ZnO nanowires. Fig. 4d reveals cross-sectional SEM images of ZnO nanowire branches grafted on magnetic cilia. It can be seen clearly that in fact the superstructure is ZnO nano-sized arrays with approximate average height of 2 μm, which greatly improve the specific surface area and contact area with incident light. Compared Fig. 4e and f, it indicates that CdS nanoparticle aggregates embellish the above branched ZnO nano-sized arrays. Because the magnetic cilia contain Co powers – a kind of magnetic material, the structure of the ZCS-B cannot be detected further to avoid damage of instrumentation system.

However, TEM can be used to reveal the atomic structure details of the ZCS-B complementally. Fig. 5a is a TEM image of representative ZnO nanowires with diameter of about 150 nm. The interplanar spacing (the insert image of Fig. 5a) is about 0.24 nm, which corresponds to the (1 0 1) plane of hexagonal ZnO [31]. After quantum dots (QDs) sensitization, the CdS QDs were coated over the ZnO branches and the average diameter of QDs is about 5–10 nm. The observed lattice fringes of 0.29 nm in the HRTEM image (the insert image of Fig. 5b) correspond to the (2 0 0) planes of CdS [32]. These results confirm that the CdS QDs have been successfully assembled on the branched ZnO nanowires arrays, so that there is a close contact between CdS and ZnO.

XRD patterns of the prepared PDMS flat sheet, ZC-B and ZCS-B films are shown in Fig. 6. The PDMS flat sheet exhibits an amorphous pattern. After grafted with ZnO nanowires, the diffraction peaks of ZnO nanowires match well with the diffraction peaks of hexagonal ZnO (JCPDS 79-2205). In the case of the ZCS-B film, there are three additional diffraction peaks at 2θ values of 26.8°, 29.2° and 38.3°, which may be ascribed to the (002), (101) and (102) crystal planes of CdS phase. The peaks of CdS on the ZCS-B film are weak, which could be attributed to its ultrane size, high dispersity and low concentration. In addition, no observable change in the ZnO crystal phase was observed after QD sensitization. Also no characteristic peaks of impurities, such as zinc nitrate, cadmium chloride, and other precursor compounds are observed.

Fig. 7 and Fig. S2 show the absorption spectra (transferred from reflectance) of magnetic cilia, ZC-B, ZC-P, PDMS flat sheet, CSC,

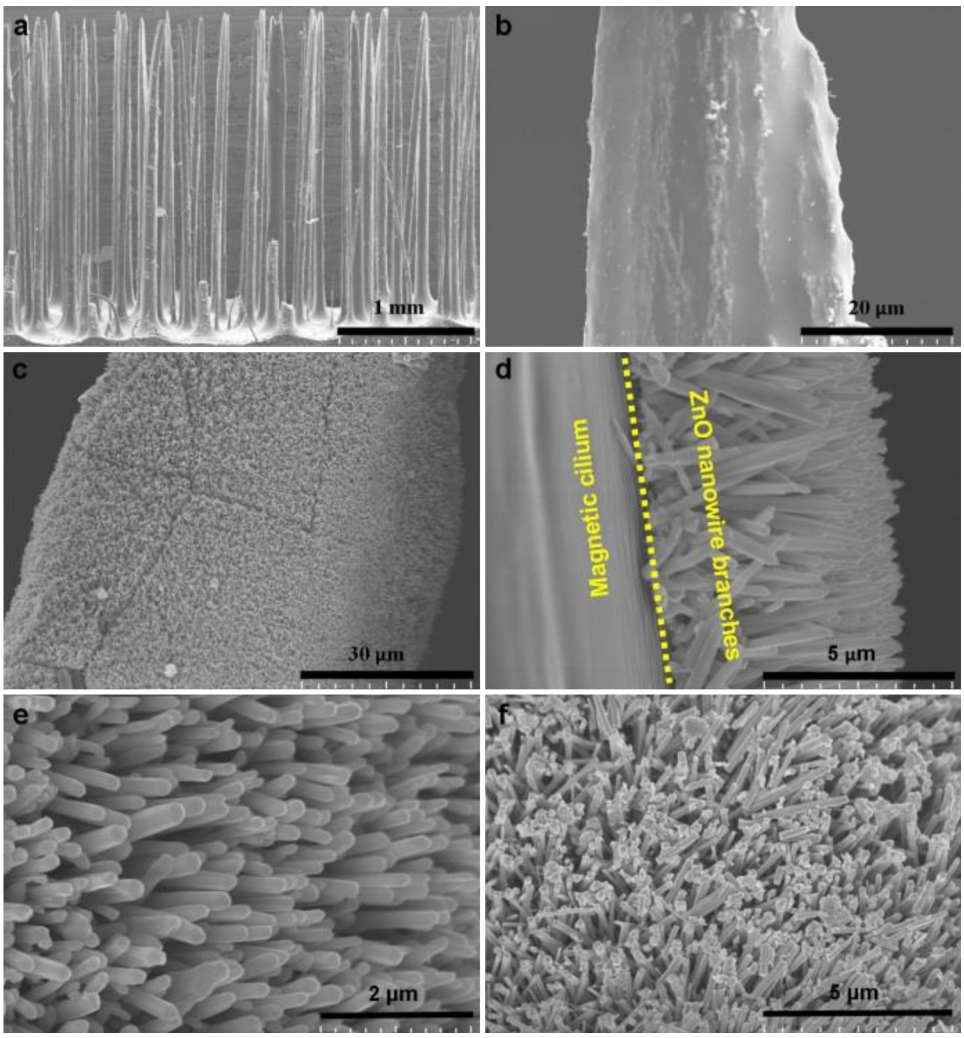

Fig. 4. FSEM images of (a) magnetic cilia, (b) a stick of magnetic cilium, (c) ZnO nanowires branches coated on a magnetic cilium, (d) cross-sectional of ZnO nanowires branches on a magnetic cilium, (e) ZnO nanowires branches (ZC-B) (top view) and (f) ZnO/CdS heterostructure (ZCS-B) (top view).

ZCS-P and ZCS-B in the range of 300–700 nm. Due to the micron-sized array structure with rough surface, magnetic cilia can scatter the incident light in all directions among cilia, resulting in long path length for efficient light usage [8,10], as shown in Fig. 7b-I. Thus, as shown in Fig. 7a and Fig. S2, the micron-sized array structure improved the light-absorption performance compared to that of the flat structure. In the case of ZnO-grafted samples, there is a great absorption in the region from 300 to 400 nm caused by the intrinsic band gap of ZnO (E_g = 3.37 eV). And a more dramatical increase occurs on ZC-B because of the structural effect of nano-sized arrays [29] (Fig. 7b-II). Compared with CSC, there is an enhanced absorption in ZCS-P and ZCS-B during the range of 300–400 nm, owing to the intrinsic property of ZnO. Most notable of all, comparison between the ZCS-P and ZCS-B demonstrates the important role of 3D branched ZnO nanowires arrays – which can effectively trap the light by extending the path length because of multiple reflection in a high density array structure [10,29,33,34] (Fig. 7b-II). Therefore, its unique micro-nano structures of the ZCS-B facilitate light

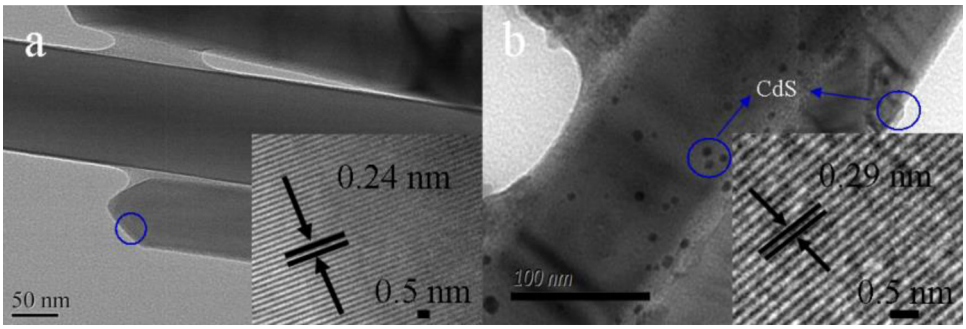

Fig. 5. (a) TEM image of ZnO nanowires and the insert image is HRTEM lattice micrograph and (b) TEM image of CdS QD-sensitized ZnO nanowires grafted on magnetic cilia and the insert image is HRTEM lattice micrograph.

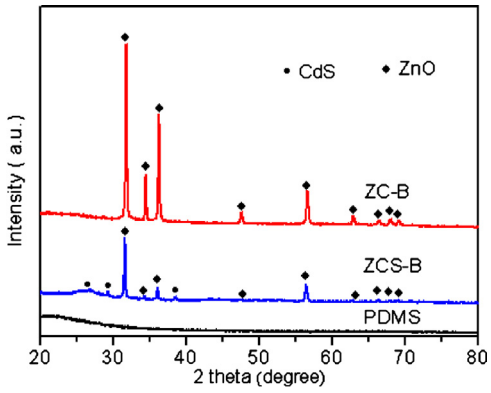

Fig. 6. Indexed XRD patterns of PDMS flat sheet, the ZC-B film and the ZCS-B film.

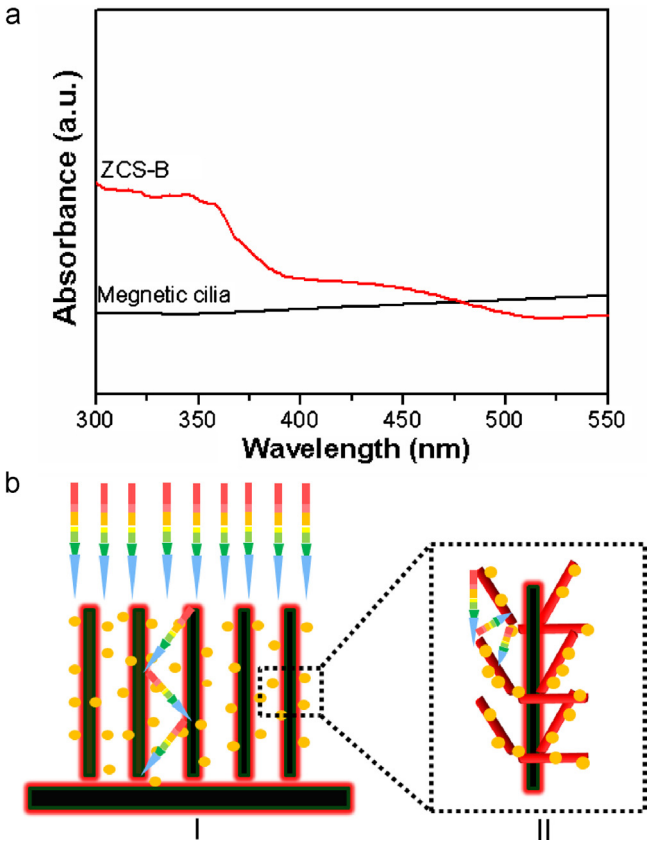

Fig. 7. (a) The absorption spectra of magnetic cilia and ZCS-B and (b) schematic illustration of the light absorption of the ZCS-B film.

absorption, which will be helpful to the performance of hydrogen evolution.

When driven to mimic ciliary motion in solution under actuation of rotational magnetic fields, the ZCS-B can move or manipulate flow like nature beating cilia. The microfluidic manipulation performance can be well regulated via tuning beating frequency of the ZCS-B, which is actually achieved by adjustment of actuation frequencies of rotational magnetic fields. In Fig. S3, the microfluidic manipulation performance of the ZCS-B was displayed in an aqueous solution (ink) under different actuation frequencies. In the actuated inner-motile ZCS-B system, the ink sparkles overlay and spreads around into the surrounding indefinitely after the ink is dropped. For being actuated at 10.5 Hz, 14 Hz and 17.5 Hz, the ink spreads into homogeneous aqueous within 12 s, 2 s and 4 s, respectively. This means the microfluidic manipulation performance is enhanced with increasing the actuated frequency, and when the actuation frequency is greater than 17.5 Hz, the microfluidic manipulation performance is still similar to that at 14 Hz. In sharp contrast, the silhouette of injected dye aqueous is still clear and hardly diffuses even within 12 s in the case of diffusive mixing process (0.0 Hz). Clearly, the actuated ZCS-B can boost fluid migration and form the flow patterns of vortical structures. The microfluidic manipulation performance can be controlled with adjusting the actuation frequency. The enhancement of the microfluidic manipulation performance through this inner-motile system provides an active transport solution that will be conducive to desorption of H_2.

It is well known that during the process of hydrogen evolution, an infinitesimal amount of H_2 is always inclined to absorb onto the surface of pholocatalyst, which may slower the evolution reaction toward hydrogen and improve the potential hazard of inverse response. However, in the inner-motile system, the release of hydrogen can be boosted via tuning beating frequency of the ZCS-B. The time from the formation of H_2 bubbles to blast is 15 s, 7.75 s and 10.5 s for being acutated at 10.5 Hz, 14 Hz and 17.5 Hz, respectively, as shown in Fig. 8. The results are consistent with that of Fig. S3, implying in a sense the enhanced microfluidic manipulation

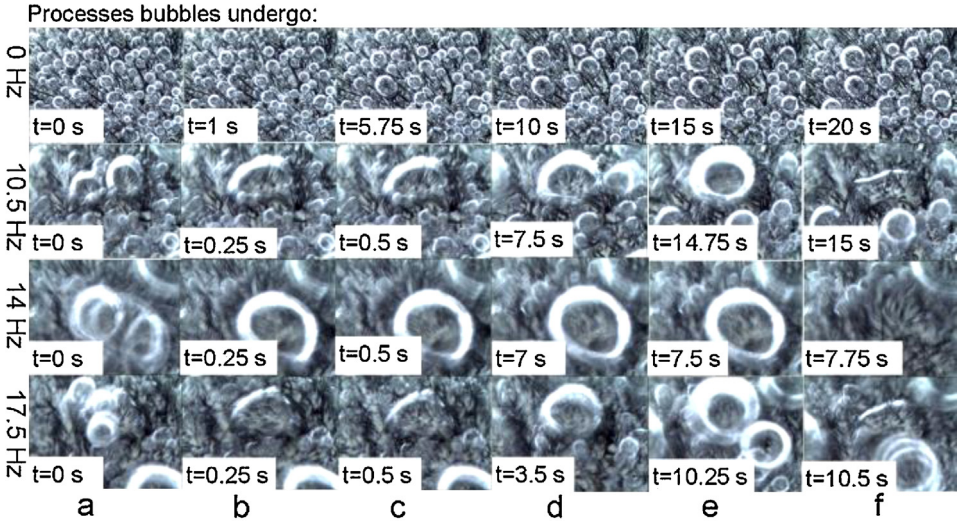

Fig. 8. Visualization of the processes in the ZCS-B system bubbles undergo in 2.5 mg/ml $NaBH_4$ solution under various actuation frequencies (0, 10.5,14, and 17.5 Hz).

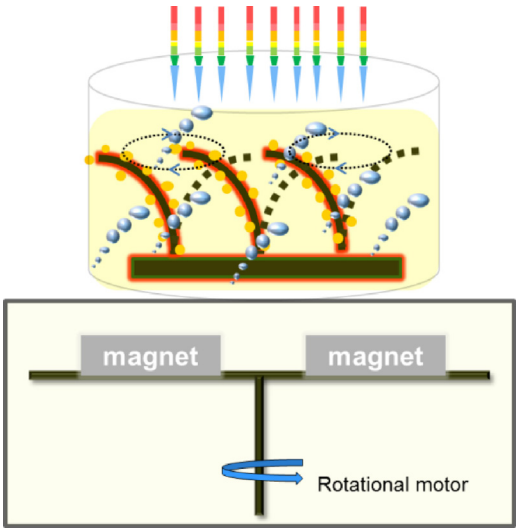

Fig. 9. schematic structure and ciliary motion of the ZCS-B film driven by a rotational magnetic field for efficient release of H_2.

performance promotes desorption of a trace of H_2 from the surface of pholocatalyst. Fig. 9 shows schematic structure and ciliary motion of the ZCS-B film driven by a rotational magnetic field for efficient release of H_2. When hydrogen is produced under illumination, the actuated inner-motile ZCS-B boosts and manipulates flow, generating induced vortices around the cilium (Fig. S3) and hence accelerating desorption and release of H_2.

The photocatalytic hydrogen evolution activity of the photocatalysts was measured as shown in Fig. 10 shown. Obviously, in Fig. 10a and b the ZCS-B holds much higher H_2 production activity than that of CSC and ZCS-P under actuation of rotational magnetic fields at actuation frequency of 14 Hz, which benefit from the ZnO/CdS coupling structure and structural effect of ZnO nanowires arrays. Based on the Z-scheme mechanism [23,27,35,36], due to the excellent carrier transport at the interface of ZnO, it was found that the photoexcited electron injection efficiency from the CBM of ZnO into the valence band maximum (VBM) of CdS was more efficient [22], hence which made ZCS-B and ZCS-P films possess much more favorable photocatalytic water splitting capability than the CSC film (Fig. 10a and b). It was acknowledged that electrons in the nanoparticles diffuse to the surface through a zigzag pathway [29], which results in the increment of electron–hole recombination, thus reducing the hydrogen production efficiency. Compared to zero-dimensional (0D) nanoparticle analogs, one-dimensional (1D) nanostructures can provide a direct rather than zigzag pathway for electron transfer. And the electron lifetime can be improved enormously through using nanowires [29]. So when excited by the incident light, excited electrons in ZnO nanowires with a lower CBM could recombine with the holes in CdS with a higher VBM through a direct pathway, more powerful excited and electrons and holes can be retained on different counterparts for efficient hydrogen production efficiency. In addition to the efficient electron transport, the nano-structure of ZnO shows pleasant structural effect. ZnO nanowires can serve as light-scattering centers to increase the optical length in the ZCS-B film, thus enhancing the light harvesting effiency (Fig. 7). So the ZCS-B shows much better performance of hydrogen production than the ZCS-P (Fig. 10a and b).

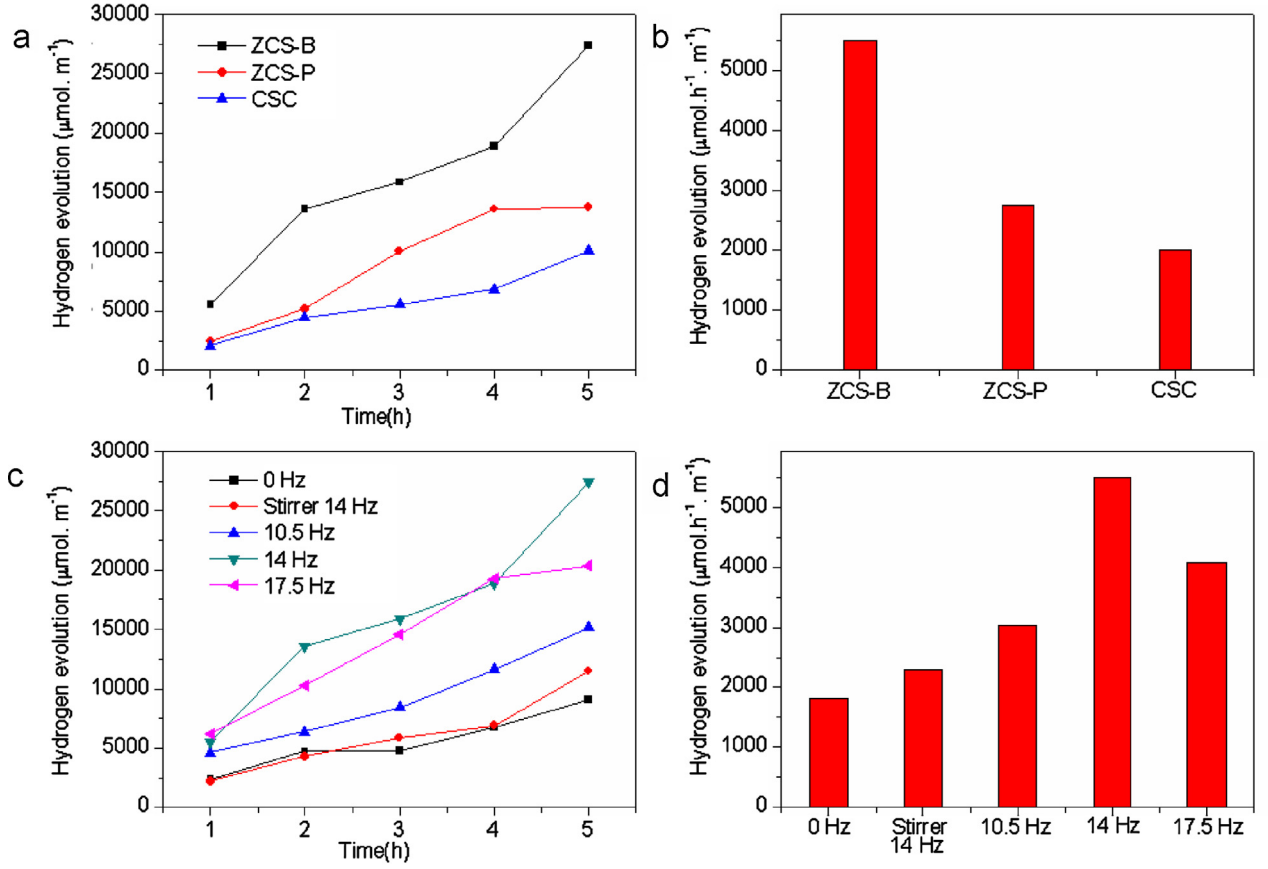

Fig. 10. (a) Photocatalytic activity and (b) average hourly hydrogen evolution rates of CSC, ZCS-P and ZCS-B for hydrogen evolution; (c) photocatalytic activity and (d) average hourly hydrogen evolution rates at different actuation frequencies in the ZCS-B system.

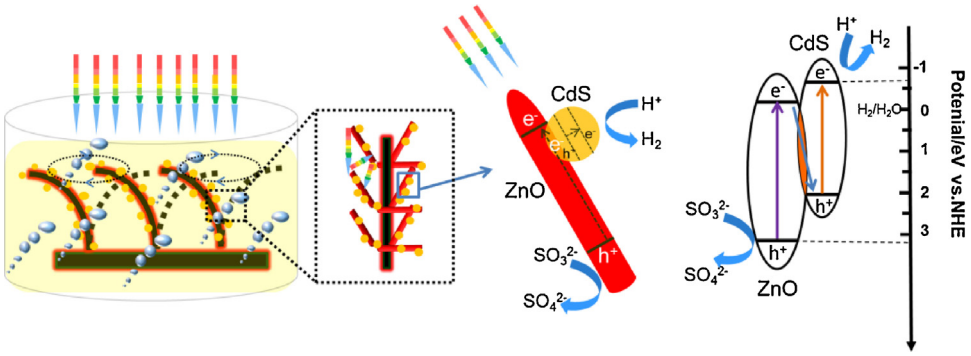

Fig. 11. Schematic illustration of the charge transfer in the Z-scheme mechanism in the inner-motile ZCS-B film for hydrogen evolution.

The ZCS-B not only processes the great superiority of structures, but also of ability to perform active microfluidic manipulation driven by rotational magnetic fields. To demonstrate the significant role of the ciliary motion, the ZCS-B was magnetically actuated at different actuation frequencies. When driven to mimick ciliary motion, the actuated ZCS-B can move or manipulate flow like nature beating cilia for desorption of H_2. In Fig. 10c and d, compared to the stationary ZCS-B (at 0 Hz), the photocatalytic activity and rate of the ZCS-B in the aid of traditional magnetic stirring with stirring bar are improved only slightly, meaning that conventional external magnetic-stirrer technologies have little help to the system of photocatalyst films. Meanwhile, through tuning the frequencies of magnetic-stirrer, the photocatalytic hydrogen evolution activity has no significant enhancement with frequencies increase, as shown in Fig. S4. This highlights the significance of designing inner inner-motile films to enhance the phtotocatalytic performance.

Meanwhile the singular inner-motile performence can be controlled by adjusting the actuation frequency of rotational magnetic fields. In Fig. 10c and d with actuation frequencies magnifying, the photocatalytic H_2 production activity and rate of the actuated ZCS-B improves. And when the actuation frequency reaches to 17.5 Hz, the activity will not improve anymore and is similar to that at 14 Hz, which is in accord with results showed in Fig. 8. It is found that the photocatalytic H_2 production activity shows a remarkable quantitative agreement with the rate of desorption of hydrogen, which are verified and powerful evidences of the importance of release of hydrogen during the photocatalytic H_2 production process. The repeated photocatalytic experiments (Fig. S5) were also conducted. It can help considerate activity.

In a word, the inner-motile 3D branched ZCS-B film can help to achieve fully efficient desorption of H_2 through serving as a local microfluidic actuator under actuation of rotational magnetic fields, making the photocatalytic activity of the ZCS-B dramatically improved.

Schematic illustration based on the Z-scheme in the ZCS system film with elaborated structures and corresponding functional modules is presented in Fig. 11. When irradiated by light, the ZCS-B film can effectively trap the light by extending the path length because of its unique micro-nano array structures. Then the photoexcited electrons in a lower CBM of ZnO nanowire inject effectively into a higher VBM of CdS through a direct pathway and recombine with the holes to realize the desirable reverse carrier transfer, so that more powerful excited electrons and holes can be retained. In addition, because the electron diffusion coefficient of ZnO nanowires is gigantic, electrons can be fast transported into CdS, which lessen recombination with holes of ZnO, and greatly prolonged lifetime of powerful excited electrons (in the CBM of CdS) and holes (in the VBM of ZnO) for the tremendous capability of hydrogen generation. During the process of hydrogen evolution, the actuated ZCS-B can move or manipulate flow for efficient desorption of H_2, avoiding reverse reaction. In short, the inner-motile ZCS films with integrated complex architecture and functional modules can work synergistically for highly efficient hydrogen production and also help to boost the desorption of H_2.

4. Conclusions

In conclusion, we innovatively explored an active and promising 3D branched ZnO/CdS heterostructures photocatalytic film, which own inner-motile system, as well as enhanced light absorption and surface area. The inner-motile ZCS-B films exhibit dramatically enhanced photocatalytic water splitting capability due to the timely desorption of H_2. The photocatalytic performance of the ZCS-B film can be controlled with adjusting the actuation frequency of rotational magnetic fields. It is worth noting that the design of ZnO nanowires branches is beneficial to enhance effective light path-length and provides fast charge transport between ZnO and CdS through a direct pathway, which is favorable for photocatalytic hydrogen generation capability. The present work may broaden the horizon for the design of artificial photocatalyst system films with synergistic functional modules and provides a novel working prototype for photochemical hydrogen production.

Acknowledgements

Financial support from the Program for Changjiang Scholars and Innovative Research Team in University (PCSIRT, IRT1146), the Jiangsu Province Postdoctoral Fund (Grant No. 1302096C), the Jiangsu Province Natural Science Foundation of China (BK20141459), the National Natural Science Foundation of China (No. 51303079), the Key University Science Research Project of Jiangsu Province (No. 10KJA430016), and a project funded by the Priority Academic Program Development of Jiangsu Higher Education Institutions (PAPD) is gratefully acknowledged.

Appendix A. Supplementary data

Supplementary data associated with this article can be found, in the online version, at http://dx.doi.org/10.1016/j.apcatb.2014.09.050.

References

[1] J. Kou, R.S. Varma, ChemSusChem 5 (2012) 2435–2441.
[2] P. Tan, J.-X. Qin, X.-Q. Liu, X.-Q. Yin, L.-B. Sun, J. Mater. Chem. A 2 (2014) 4698.
[3] Z. Li, Y. Luan, Q. Wang, G. Zhuang, Y. Qi, Y. Wang, C. Wang, Chem. Commun. (2009) 6273–6275.
[4] A. Kargar, K. Sun, Y. Jing, C. Choi, H. Jeong, Y. Zhou, K. Madsen, P. Naughton, S. Jin, G.Y. Jung, D. Wang, Nano Lett. (2013).
[5] Q. Tang, W. Zhou, J. Shen, W. Zhang, L. Kong, Y. Qian, Chem. Commun. (2004) 712–713.

[6] C. Wen, F. Liao, S. Liu, Y. Zhao, Z. Kang, X. Zhang, M. Shao, Chem. Commun. 49 (2013) 3049–3051.
[7] D. Buso, J. Pacifico, A. Martucci, P. Mulvaney, Adv. Funct. Mater. 17 (2007) 347–354.
[8] K. Sun, Y. Jing, C. Li, X. Zhang, R. Aguinaldo, A. Kargar, K. Madsen, K. Banu, Y. Zhou, Y. Bando, Z. Liu, D. Wang, Nanoscale 4 (2012) 1515–1521.
[9] R. Portela, S. Suárez, R.F. Tessinari, M.D. Hernández-Alonso, M.C. Canela, B. Sánchez, Appl. Catal. B: Environ. 105 (2011) 95–102.
[10] A.B. Yun Jeong Hwang, P. Yang, Nano Lett. 9 (2008) 410–415.
[11] G. Li, B. Sun, Y. Wang, Z. Wu, W. Zhang, Int. J. Photoenergy 2014 (2014) 1–5.
[12] G. Li, Z. Yi, Y. Bai, W. Zhang, H. Zhang, Dalton Trans. 41 (2012) 10194–10198.
[13] G. Li, Z. Yi, H. Wang, C. Jia, W. Zhang, Appl. Catal. B: Environ. 158–159 (2014) 280–285.
[14] M.G.H.M.B.S.N. Khaderi, P.D. Anderson, D. Ioan, J.M.J. den Toonder, P.R. Onck, J. Mech. Phys. Solids (2009).
[15] J.M.J. den Toonder, P.R. Onck, S.N. Khaderi, J. Fluid Mech. 688 (2011) 44–65.
[16] S.N. Khaderi, C.B. Craus, J. Hussong, N. Schorr, J. Belardi, J. Westerweel, O. Prucker, J. Ruhe, J.M. den Toonder, P.R. Onck, Lab Chip 11 (2011) 2002–2010.
[17] J.M. den Toonder, P.R. Onck, Trends Biotechnol. 31 (2013) 85–91.
[18] F. Fahrni, M.W. Prins, L.J. van Ijzendoorn, Lab Chip 9 (2009) 3413–3421.
[19] C.Y. Chen, C.Y. Chen, C.Y. Lin, Y.T. Hu, Lab Chip 13 (2013) 2834–2839.
[20] C.J. Jaakko, V.I. Timonen, K. Kontturi, A. Walther, O. Ikkala, R.H.A. Ras, ACS Appl. Mater. Interface 2 (2010) 2226–2230.
[21] Z. Dunpu, W. Wei, P. Fengping, K. Jiahui, N. Yaru, L. Chunhua, X. Zhongzi, Nanoscale (2014).
[22] X. Wang, G. Liu, Z.G. Chen, F. Li, L. Wang, G.Q. Lu, H.M. Cheng, Chem. Commun. (2009) 3452–3454.
[23] A. Iwase, Y.H. Ng, Y. Ishiguro, A. Kudo, R. Amal, J. Am. Chem. Soc. 133 (2011) 11054–11057.
[24] Y. Sasaki, H. Kato, A. Kudo, J. Am. Chem. Soc. 135 (2013) 5441–5449.
[25] S.S. Ma, K. Maeda, T. Hisatomi, M. Tabata, A. Kudo, K. Domen, Chemistry 19 (2013) 7480–7486.
[26] H. Kato, Y. Sasaki, N. Shirakura, A. Kudo, J. Mater. Chem. A 1 (2013) 12327.
[27] H. Zhou, L. Ding, T. Fan, J. Ding, D. Zhang, Q. Guo, Appl. Catal. B: Environ. 147 (2014) 221–228.
[28] H. Zhou, X. Li, T. Fan, F.E. Osterloh, J. Ding, E.M. Sabio, D. Zhang, Q. Guo, Adv. Mater. 22 (2010) 951–956.
[29] Y. Bai, H. Yu, Z. Li, R. Amal, G.Q. Lu, L. Wang, Adv. Mater. 24 (2012) 5850–5856.
[30] C.L.D. Xu, D. Zhang, J. Song, Y. Ni, Z. Xu, Mater. Lett. 71 (2012) 94–97.
[31] C.K. Xu, G.D. Xu, Y.K. Liu, G.H. Wang, Solid State Commun. 122 (2002) 175–179.
[32] F. Su, J. Lu, Y. Tian, X. Ma, J. Gong, Phys. Chem. Chem. Phys. 15 (2013) 12026–12032.
[33] J.-H. Yoon, S.-R. Jang, R. Vittal, J. Lee, K.-J. Kim, J. Photochem. Photobiol. A: Chem. 180 (2006) 184–188.
[34] M.K. Nazeeruddin, R. Splivallo, P. Liska, P. Comte, M. Grtzel, Chem. Commun. (2003) 1456.
[35] H. Kato, Y. Sasaki, A. Iwase, A. Kudo, Bull. Chem. Soc. Jpn. 80 (2007) 2457–2464.
[36] H. Zhu, B. Yang, J. Xu, Z. Fu, M. Wen, T. Guo, S. Fu, J. Zuo, S. Zhang, Appl. Catal. B: Environ. 90 (2009) 463–469.